REPORT DOCUMENTATION PAGE

Form Approved
OMB No. 0704-0188

1. AGENCY USE ONLY (Leave blank)	2. REPORT DATE	3. REPORT TYPE AND DATES COVERED
	4 January 1995	FINAL, 1 Sep 93 to 31 Aug 94

4. TITLE AND SUBTITLE

LOW ORDER ADAPTIVE OPTICAL SYSTEMS

5. FUNDING NUMBERS

6. AUTHOR(S)

J C DAINTY and A KORYABIN

7. PERFORMING ORGANIZATION NAME(S) AND ADDRESS(ES)

Imperial College of Science, Technology and Med,
Blackett Laboratory,
Prince Consort Road,
LONDON SW7 2BZ, UK.

8. PERFORMING ORGANIZATION REPORT NUMBER

9. SPONSORING/MONITORING AGENCY NAME(S) AND ADDRESS(ES)

EOARD/LRP,
223-231 Old Marylebone Road,
London NW1 5TH, UK

10. SPONSORING/MONITORING AGENCY REPORT NUMBER

TR 95-03

11. SUPPLEMENTARY NOTES

12a. DISTRIBUTION/AVAILABILITY STATEMENT

Approved for public release;
distribution unlimited

12b. DISTRIBUTION CODE

13. ABSTRACT (Maximum 200 words)

This Report presents the evaluation results of the performance of a bimorph piezoelectric mirror supplied by the International Laser Center. The first part describes the spatial modes of the mirror, their linearity, hysteresis and their temperature dependence. The next part describes the dynamic behaviour.

The final part of the report presents results of the performance of a simple adaptive optical system for imaging through laboratory generated turbulence. The mirror and system might be suitable for low order correction in a 1m - class telescope.

14. SUBJECT TERMS

Adaptive optics, Imaging.

15. NUMBER OF PAGES
35 + cover

16. PRICE CODE

17. SECURITY CLASSIFICATION OF REPORT	18. SECURITY CLASSIFICATION OF THIS PAGE	19. SECURITY CLASSIFICATION OF ABSTRACT	20. LIMITATION OF ABSTRACT
Unclassified	Unclassified	Unclassified	

TR-95-03

This report has been reviewed and is releasable to the National Technical Information Service (NTIS). At NTIS it will be releasable to the general public, including foreign nations.

This technical report has been reviewed and is approved for publication.

VICTORIA H. COX
Chief, Physics and BMD Coordinator

for DONALD R. ERBSCHLOE, Lt Col, USAF
Chief, International Programs

TR-95-03

Low Order Adaptive Optical System

Abstract

The report represents the evaluation results of the performance of the bimorph piezoelectric adaptive mirror. The first part of results concerns spatial modes of the mirror, their linearity, hysteresis and their temperature dependence. The next part of results concerns the dynamic behaviour of the mirror.

The last part of the report represents results of the performance of the simple adaptive optical system for imaging through laboratory generated turbulence. In conclusion we presented the general evaluations of the adaptive optical system with bimorph mirror for 1m class telescope.

Contents

1. Bimorph piezoelectric deformable mirror.

1.1. The progress in adaptive optics (AO) application is mainly associated with increasing the number of controlled subapertures and feedback control circuits. As a result of such development there appeared systems with more than 200 subapertures and the plan was reported to built 490 subapertures AO telescope [1]. There are two major problems on this way. First, it leads to increasingly high cost of AO systems. Second - the higher the order of correction required (this broadly equals the number of the mirror actuators), the more light you need to get accurate measurements of the distorted wavefront.

One way to overcome these problems is to use a rather small number of active subapertures for on-line real time pre-processing of the observed image and to optimise parameters of AO system to achieve effectiveness required for post-processing.

In experiments on AO phase correction, performed in MSU since 1979, we used bimorph deformable mirrors (BDM) with comparatively small number (from 8 to 17) of actuators or spatial deformation modes as key elements. A number of papers were published on specific problems concerning such DM applications:

- parameters optimisation and design [2];
- measurements of operating parameters [3];
- computations of effectiveness in different adaptive systems [4].

A number of laboratory experiments were performed on BDM applications. Results obtained revealed sufficiently high effectiveness of bimorph mirrors to compensate low order aberrations such as thermally induced distortions in laser systems [5,6]. The last reports by other groups show the wide interest for BDM astronomical application as, for example - COME ON PLUS and CFH projects [6].

1.2. The concept of BDM has been suggested in [7] and at first realised by Lipson and Steinhaus [8]. The device (see fig 1.1) consists of a glass plate firmly glued to a plate actuator disc, made from piezoelectric ceramic. In our BDM the actuator disc on its turn consists of two piezoceramic discs (lead zirconium titanate), soldered together and polarised normally to their surfaces.

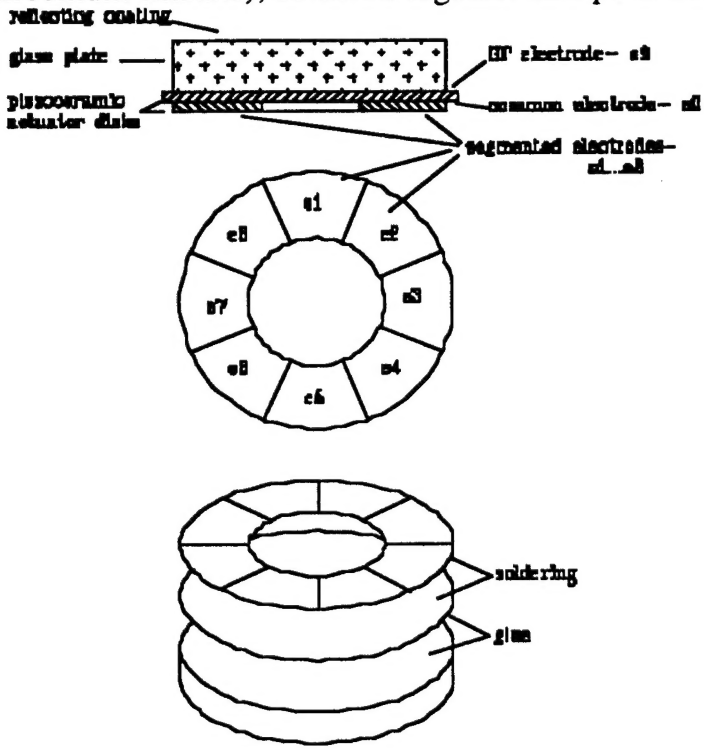

Fig. 1.1 Bimorph adaptive mirror

The diameter of the glass plate is 39 mm and thickness 4 mm. The active surface of the plate has reflecting aluminium layer with protecting SiO_2 cover. The thickness of each piezoceramic disc is 0.35 mm.

The interface between the two discs contains continuos conducting electrode - we shall call it "ground electrode". The second continuos conducting electrode between the actuator and the glass plate is used to control the curvature of the whole mirror and we shall call it "general focus electrode". The outer surface of the actuator has 8 separate ring-segment electrodes to control mirror's astigmatism.

The mirror profile dependence via control voltages applied to electrodes can be described by Poisson equation [8,9].

1.3. In the experiments presented we used two mirrors (fig. 1.2). One mirror was fixed to the mount by a glass tube attached to the actuator disc. We'll call it BDM1 - "fixed centre mirror". The second mirror was fixed to the mount

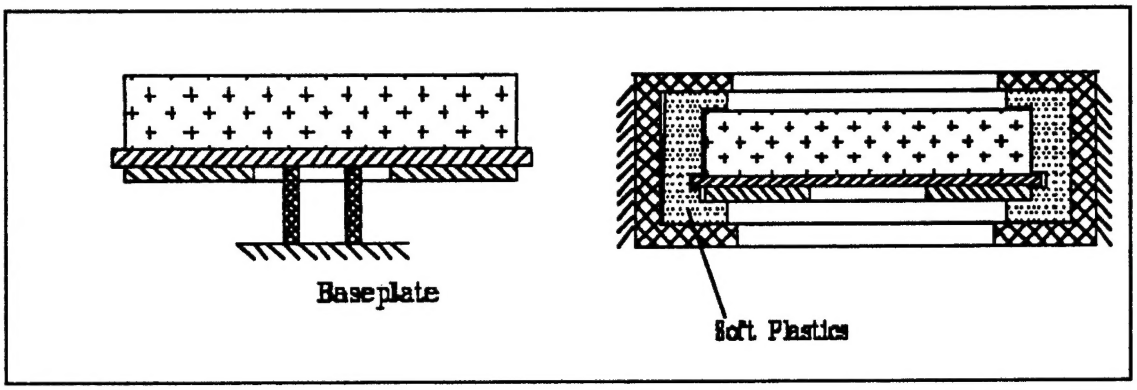

Fig.1.2. Mirror attachment variants:
fixed centre (left), quasi-free mirror

by a soft plastic bandage. We'll call it BDM2 - "quasi free mirror". The BDM1 mount has no tip-tilt actuators so we should use separate plate mirror for tip-tilt control. Actually it's not a disadvantage, because any modern telescope has a separate precise tracking system. Moreover, the fixed centre mirror can be built in the AO set-up more precisely, than quasi free mirror.

The BDM2 hold mount can be attached to the tip-tilt controlled mount. This mount has 2 PZT stick actuators with 2.5 μm stroke at 300 V drive that allows us to get about 5 mrad tip-tilt control range.

Due to the large capacitance of actuators and the relatively high weight of the attached BDM2 holder mount the dynamic parameters of the configuration are rather poor - it has less than 100 Hz frequency bandwidth.

The tip-tilt controlled mount can be used for angular correction separately by attachment of a small (up to 25 mm) plate mirror. This configuration allows to obtain 1.2 KHz bandwidth that is quite enough for astronomical turbulence compensating systems.

2. Spatial parameters of the mirror

Practically all results presented in this section concerns the BDM1 - fixed centre mirror. Spatial parameters of the BDM2 have been completely measured previously in MSU. Shortly we can summarise that the second order aberrations may be fitted with RMS error about 6% and max p-p aberration value is 4 μm at 300 V. The first resonance frequency was about 1-1.2 KHz and active bandwidth is about 500-600 Hz.

2.1. ***Interferometer***. Spatial parameters of mirrors were measured on commercial digital phase shifting Moller-Wedel interferometer with Phase Shift Technology software. The main operating parameters of the interferometer:

Phase measurement resolution - $\lambda/256$ (λ=0.63μm);

Phase measurement accuracy better than $\lambda/50$ p-p;

Repeatability better than $\lambda/100$;

Data acquisition time less than 1 second;

Fitting of phase data to 36 Zernike polynomials.

Data obtained on the interferometer can be stored in three file formats: INT - for intensity, MAP - for phase profile, and ZRN - for Zernike representation. Application software to convert this data into standard BMP and ASCII-DAT file formats was written using Borland Turbo Pascal 7.0. The most part of results is presented in terms of Seidels aberrations.

To control BDM aberrations we used the handle control unit, that consists of 6 potentiometers and 2 DC voltage converters - from +12V to

+300V and from +12V to -300V DC. Output voltages of this unit can varies from -150 V to +150 V.

2.2. *Low order aberrations fitting. Hysteresis.*

2.2.1. *Plane fitting*. The interferogram and spatial profile of the mirror with zero control voltages, measured at 18°C, are shown at fig.2.1. The main initial

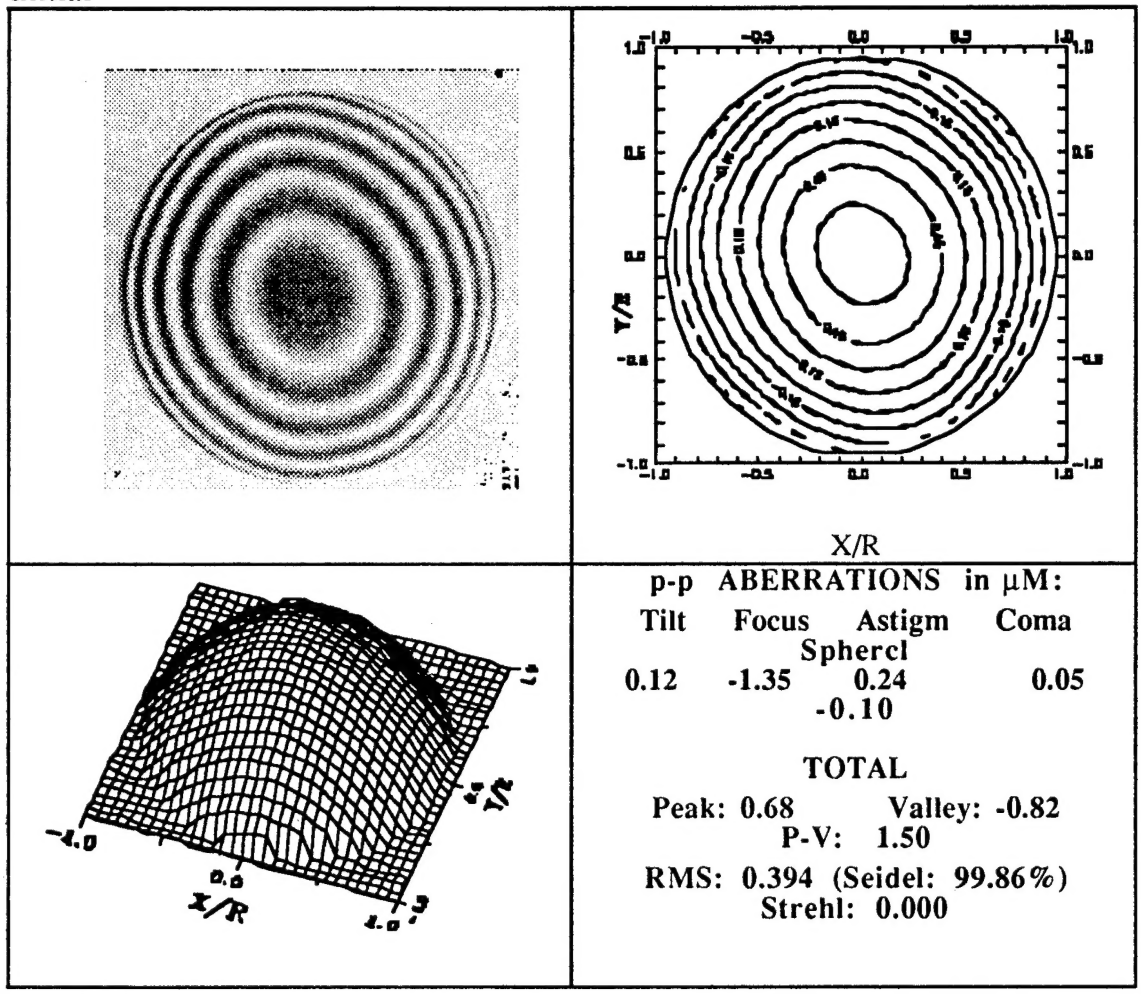

Fig.2.1. The profile of the mirror at zero control voltages

aberrations are general focus - 1.35 μm (p-v), astigmatism - 0.24 μm, and spherical 0.1 μm, the last one is mostly due to the centre fixing rod influence. Average RMS value of aberration was 0.394 μm, and the most part of it -

99.86%, was represented by Seidel aberrations: defocus, astigmatism, pure coma and spherical.

We connected the opposite segmented electrodes of the mirror so we applied one control voltage to e1&e5 electrodes pair, the next control voltage to e2&e6 pair and so on. By handle control of these 5 voltages (one for general focus electrode) we succeeded to obtain plain fitting with 0.169 μm p-p and 0.033 μm RMS aberration - fig.2.2. Control voltages for this case are represented in Table 2.1.

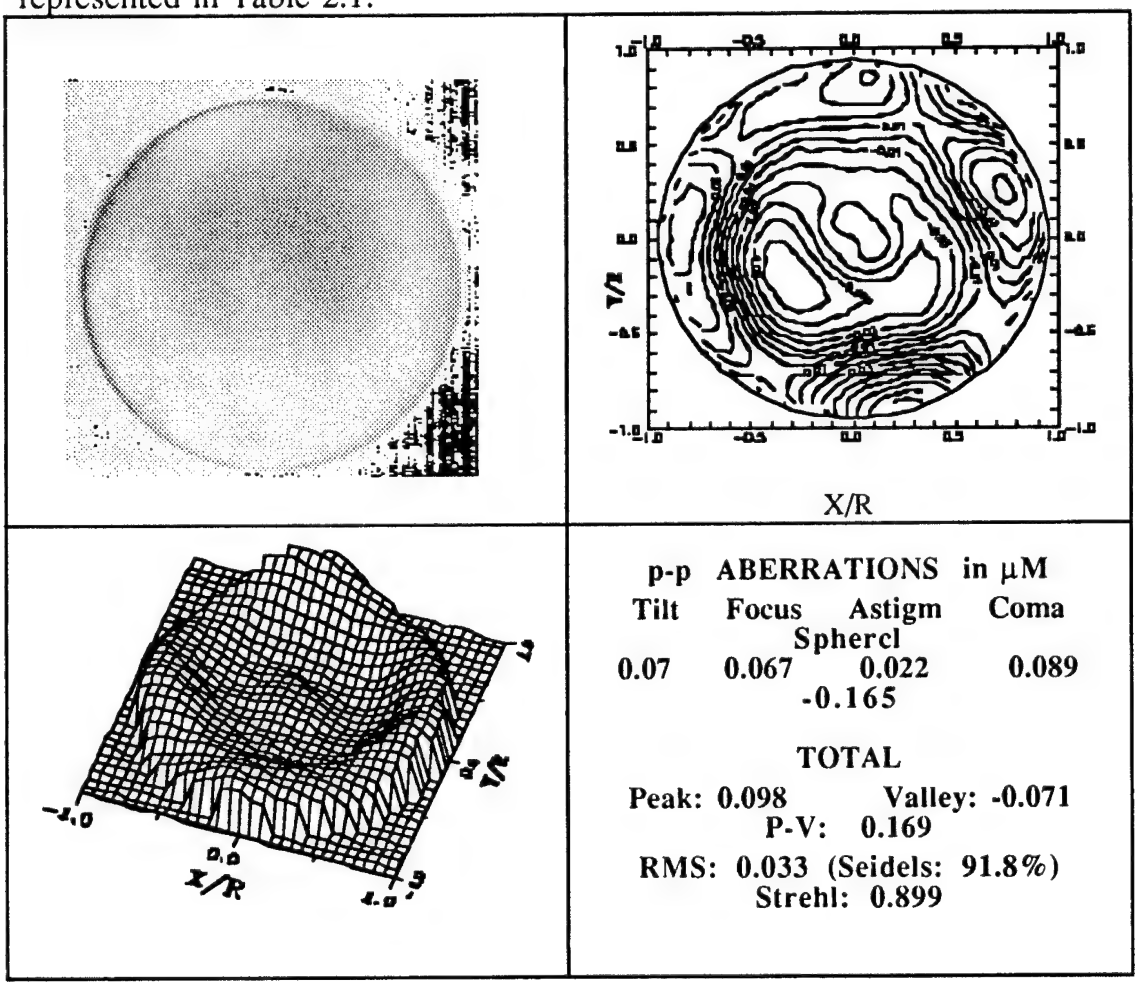

Fig.2.2. Plane fitting by 5-channels handle control

Table 2.1. Control voltages for plane fitting.

e1=e5	e2=e6	e3=e7	e4=e8	e9
5.6	-9.2	-2.3	16.4	-42

The maximum voltage -42V was applied to electrode e9 (general focus electrode) to compensate initial defocus of the mirror. For the computer controlled closed loop adaptive system with a wave front sensor we may hope to obtain the fitting of plane with less RMS error.

2.2.2. *General focus control.* The dependance of the Seidel aberrations via the closed cycle of the e9 control voltage variation are represented at fig.2.3 (general focus) and 2.4.(astigmatisms, coma and spherical aberrations). The curve at fig.2.2 shows high controllability of the mirror by general focus electrode: the amplitude of general focus variation 6.28 μm at 245 V control voltage variation. These figures gave us the next value of the control gain coefficient k_F:

$k_F = \Delta F/\Delta V = 0.0256\ \mu M/V.$

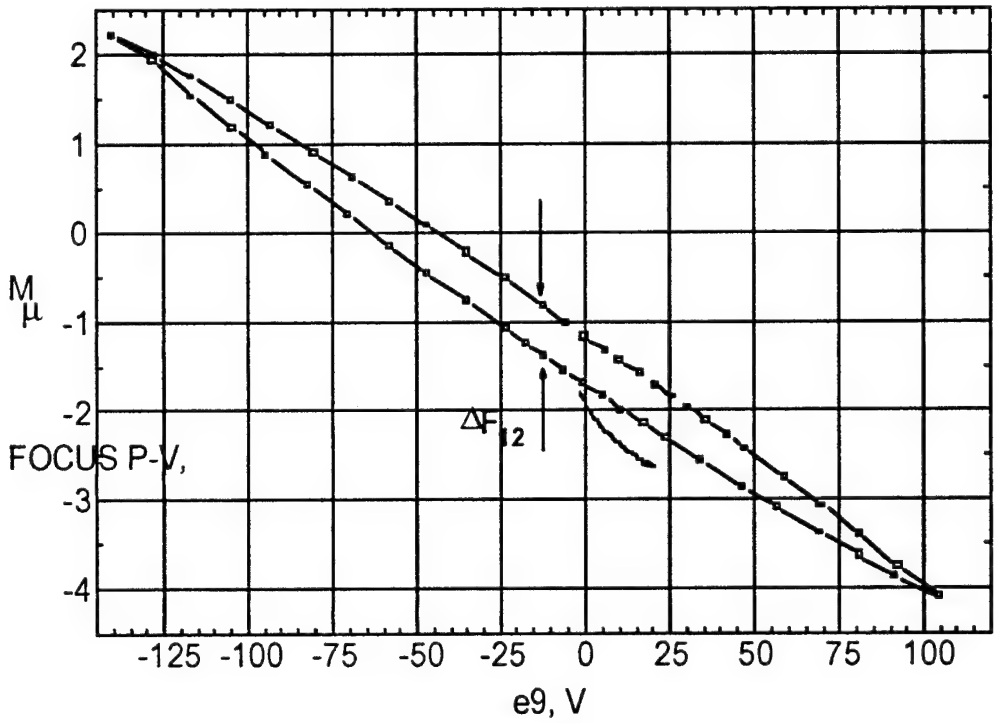

Fig.2.3. General focus control by the e9 electrode.

These results reveals the typical influence of the PZT ceramic hysteresis, for general focus aberration the absolute value of the width $\Delta F_{12}$of the hysteresis curve was 0.56μM which corresponded to the relative value δ_F = 8.9%. In closed control circuite the influence of hysteresis can be significantly decreased by additional feedback loop [12]. Control gain coefficients for Seidel aberrations are shown in table 2.2.

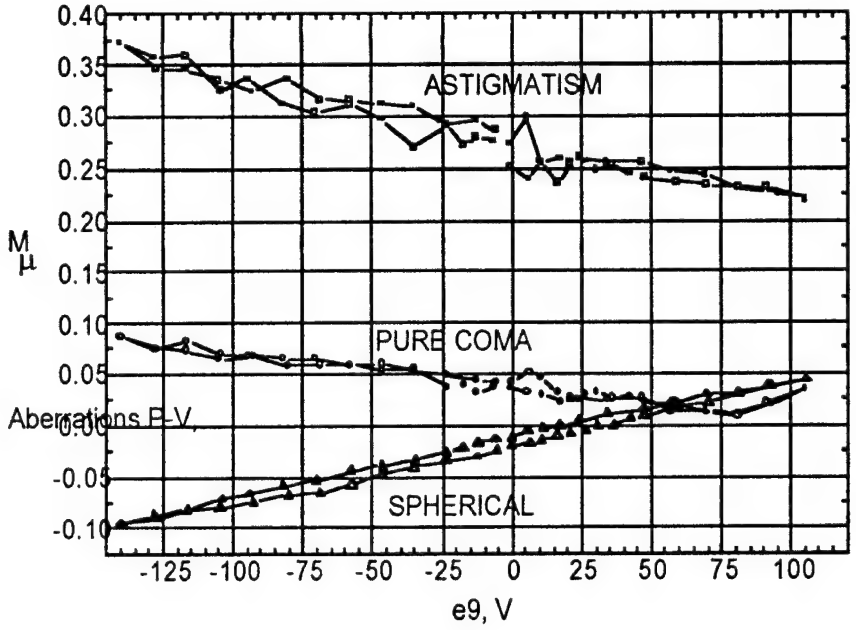

Fig.2.3. Seidel aberrations for general focus (e9) control.

Table 2.2. Control gain coefficients for e9 general focus control.

Aberration	astigmatism	coma	spherical
control gain, x10^4 μM/V	-6.1	-3.6	5.7

The similar curves (see fig.2.4, 2.5) were obtained for general focus control by applying the same voltages to all segmented electrodes - e1..e8. As it could be expected the control gain coefficient k_F was almost 2 times less in compare with the previous case (control by electrode e9):

$k_F = \Delta F/\Delta V = 0.0112$ μM/V.

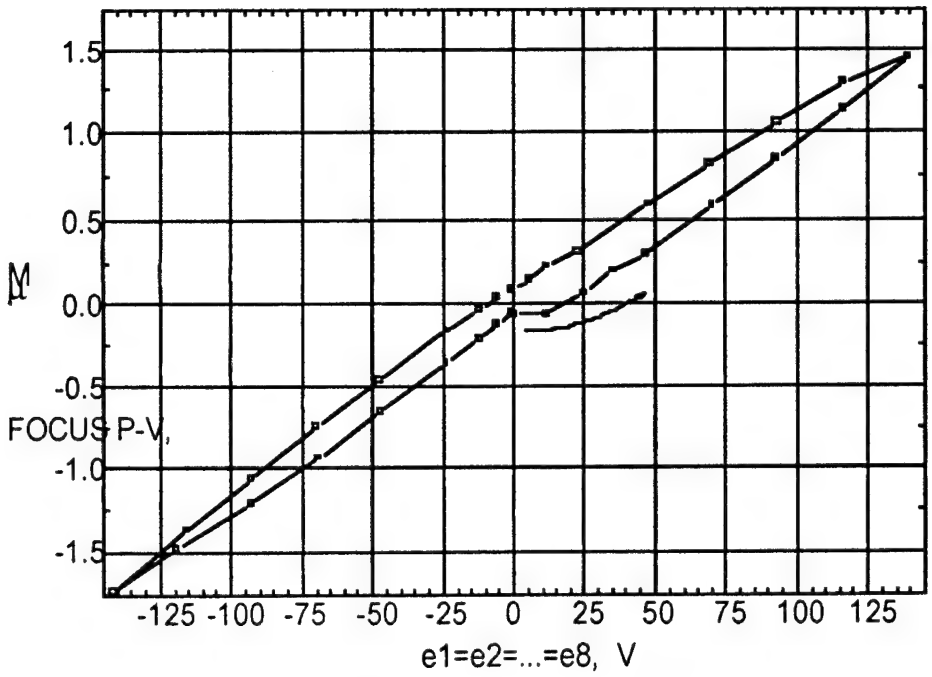

Fig.2.4. General focus control by segmented electrodes.

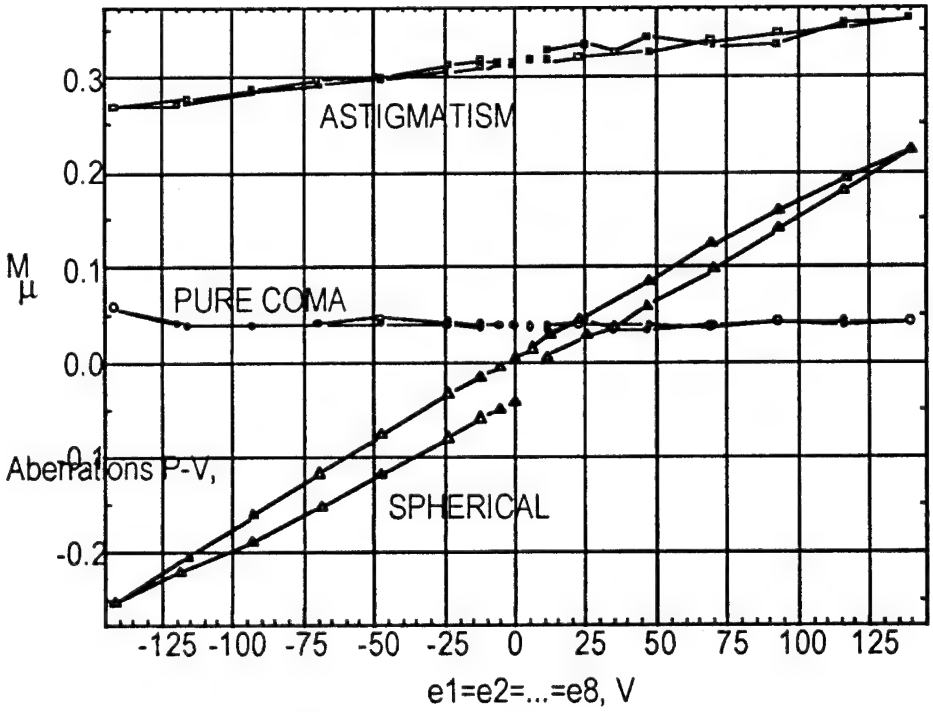

Fig.2.5. Seidel aberrations for general focus (e1-e8) control.

Control gain coefficients for Seidel aberrations for segmented electrodes control are shown in table 2.3.

Table 2.3. Control gain coefficients for e1-e8 general focus control.

Aberration	astigmatism	coma	spherical
control gain, $x10^4$ μM/V	-3.4	-0.57	16.7

2.2.3. *Spherical aberration.* The significant difference in the control gain coefficients of the spherical aberration for e9 and e1-e8 cases gives us possibility to control this aberration by applying a certain voltage difference between e9 electrode and the ring of segmented electrodes. The results for spherical aberration control are shown at fig.2.6 - spherical aberration and fig.2.7 - astigmatism, coma and focus. At fig.2.6 horizontal axis represents segmented electrodes voltage and corresponding e9 voltage values are shown near experimental points. Control gain coefficient for spherical aberration had the value $1 \cdot 10^{-3}$ mM/V.

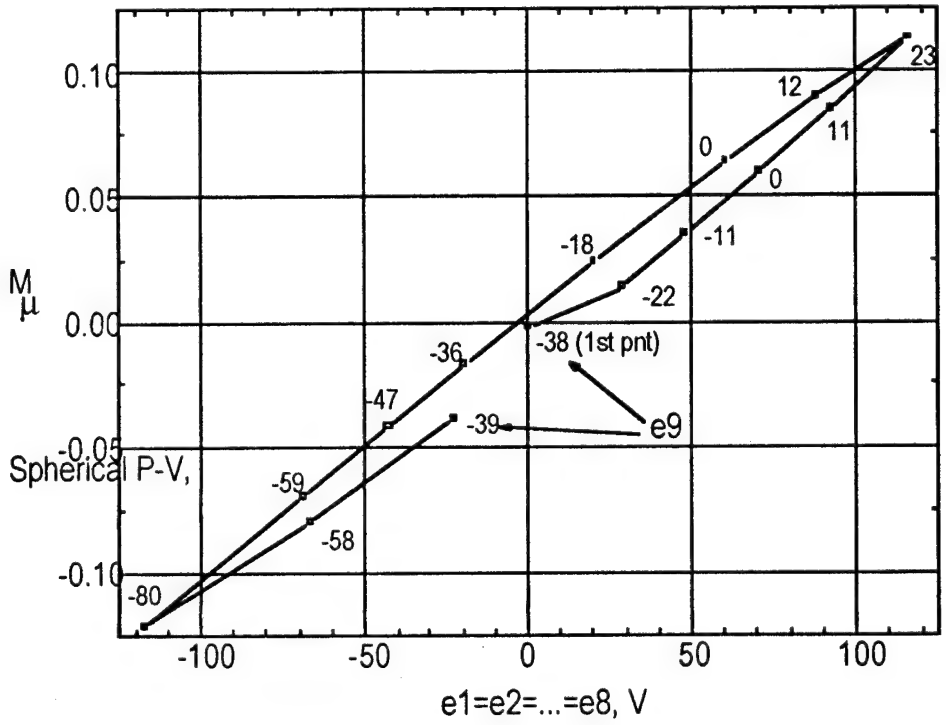

Fig.2.6. Spherical aberration control.

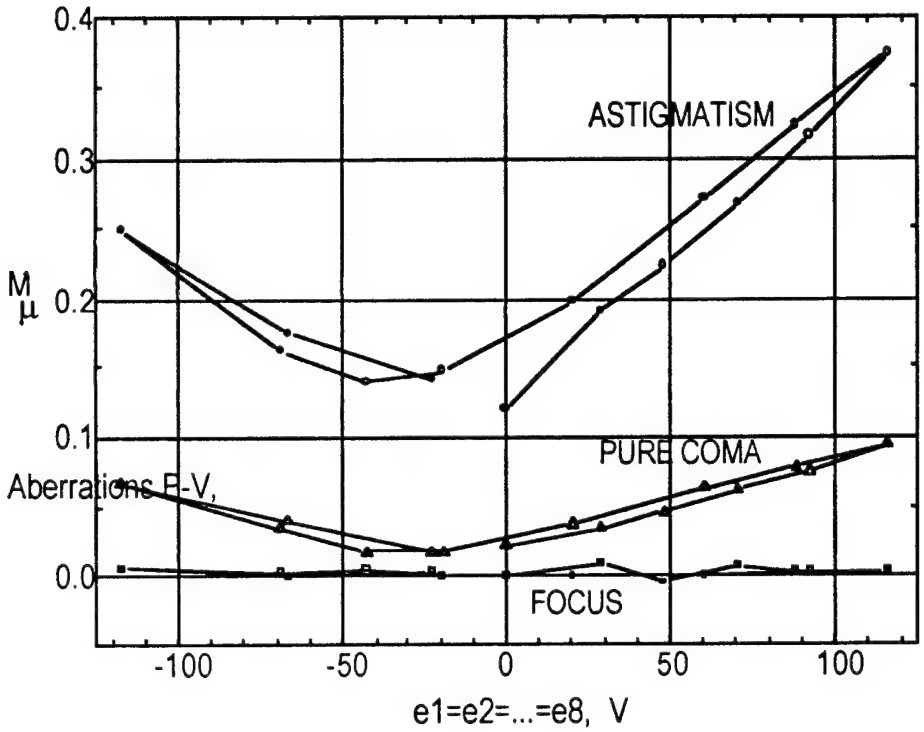

Fig.2.7. Sedel aberrations (exl. spherical) for spherical aberration control.

Negligible values of general focus aberration (fig.2.7) proves that we imposed correct differences between e9 and e1-e8 voltages. The significant variations of astigmatism in this case can be explained by a certain misalignment between the centre of the mirror plate and the centre of fixation rode as well as by imperfection of electrodes geometry.

2.2.4. *Astigmatism.* To control astigmatism we applied a certain positive voltage to a pair of opposite segmented electrodes and the same negative voltage to another pair of electrodes, as it shown at fig.2.8. To compensate the initial defocus we applied 20.2V to the e9 electrode. Axes of maximum deformation for this case almost coincided the X-Y axes and in terms of Seidels we can call this aberration 2^{o}-astigmatism. The control gain coefficient for this case had the value $k_{ast}=2.2\cdot10^{-2}$ μm/V.

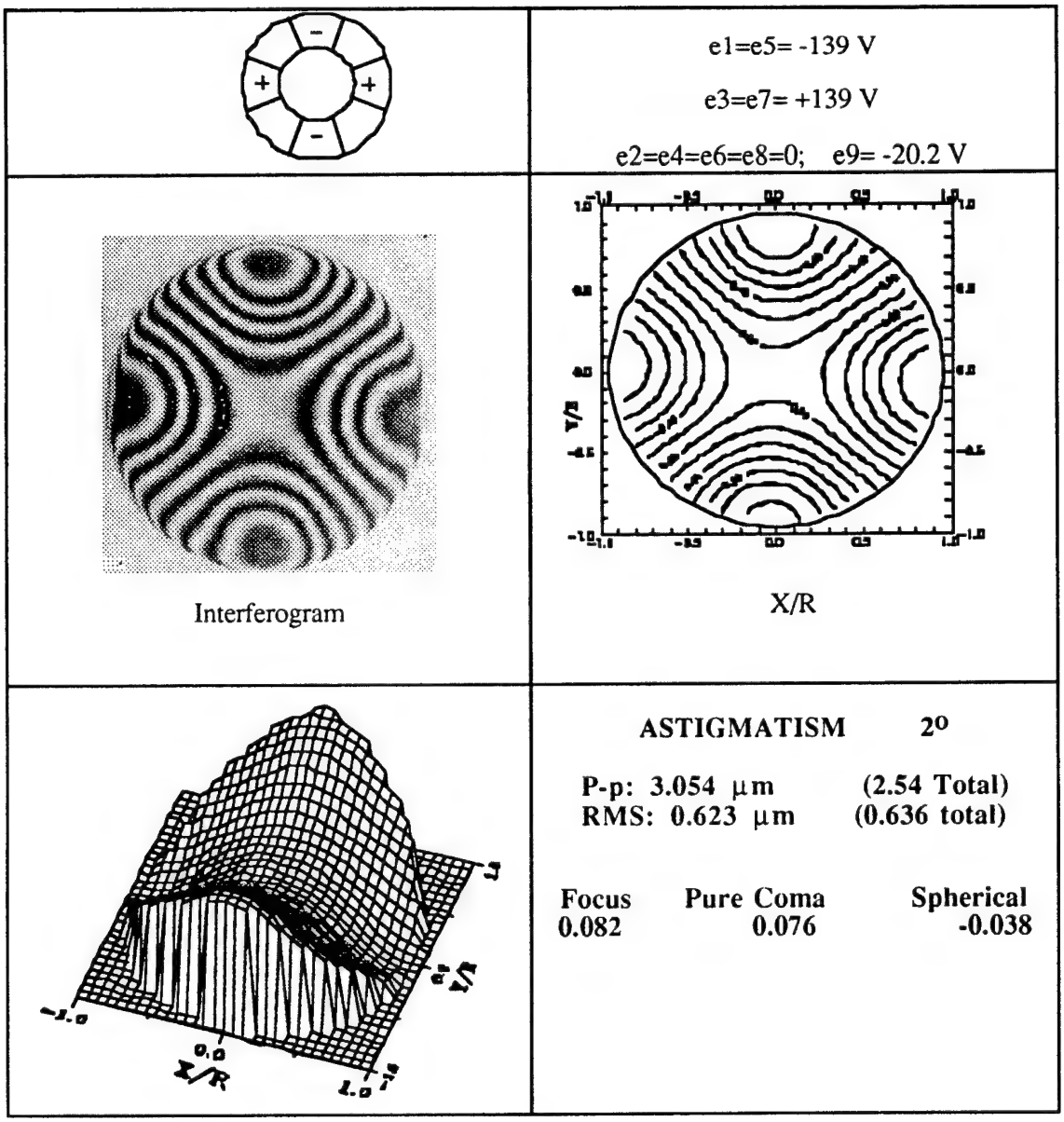

Fig.2.8. Astigmatism fitting results.

The similar results for reversed signs of control voltages gave us the value of k_{ast}=1.95 10^{-2} μm/V. To obtain 45°-astigmatism we applied +139V to electrodes e4,e8 and -139V to electrodes e2,e6. The control gain coefficient k_{ast}. for this case had the value 1.88 10^{-2}μm/V and 2.23 10^{-2} μm/V for reversed signes of applied voltages.

2.2.5. *Coma*. Originally this mirror with 8 segmented electrodes wasn't designed to correct the coma aberration. As it was difficult to fit the coma by handle control of 6 voltages available the next procedure was used. For every segmented electrode we measured the response profile and their Zernike expansions (36 terms) were used to calculate the accuracy of the lowest aberrations fitting by LSE method. The results of these calculations are represented in table 2.4 (fitting errors) and 2.5 (control voltages).

Table 2.4. Calculated Errors of the lowest Zernike Fitting

Aberration	*P-to-V, μM*	*RMS, μM*	*RMS/P-V, %*
Plane	-	0.0315	
Focus	1.27	0.0076	0.6
Astigmatism 1	1.27	0.037	2.9
Astigmatism 2	1.27	0.038	3.1
Pure Coma 1	1.27	0.06	4.8
Pure Coma 2	1.27	0.2	15
Spherical	0.949	0.28	30

Table 2.5. Calculated Control Voltages to fit the lowest Zernike, V

Aberration	*e1*	*e2*	*e3*	*e4*	*e5*	*e6*	*e7*	*e8*	*e9*
Plane	6.2	-20	-6.8	16.4	16.7	7.	-7.1	8.2	8
Focus	5.9	6	6.1	5	5.5	6	10.7	3.9	-42.2
Astigm. 1	31.4	5.3	-28.8	0.7	33.9	5	-24.8	3.8	3.8
Astigm. 2	0.5	31.8	9.4	-32.9	-7.6	26.5	3.8	-30.2	-0.4
Pure Coma 1	10.2	-86.8	-132	-89.3	-34.2	54.4	80	64.1	-19.7
Pure Coma 2	30.4	24.9	9.2	-16.4	-28.8	-15.3	-2.7	22.1	3.7
Spherical	5.4	9.3	15.7	9.8	1	-5.1	-7.3	-6.1	3.7

In accordance with the results presented in tab.2.4 while one type of the coma - "pure coma 1" can be fitted with RMS error less than 5%, another one - pure coma 2 has significantly higher fitting error - 15% in term of RMS. The fitting error value obtained for spherical aberration is about 30%. At the same time fitting errors for the second order aberrations, for which this mirror was designed, are about 3% for astigmatism and 0.6% for defocus.

2.2.6. *Estimations for turbulence correction application.* For general estimation of the mirror effectiveness in astronomical AO system we can use results obtained by R.J.Noll [9]. He calculated weights of Zernike aberrations

in wavefront distortions caused by Kolmogorov's type turbulence. These low aberrations weights in the total phase variance σ^2_Φ on a circular aperture D are represented in table 2.6. In the table 2.7 the figures of the vision quality in terms of the Strehl coefficient S are represented for a number of D/r_0 values (r_0 - wavefront coherence length).

Table 2.6. Low order aberrations percentage in the total phase variance σ^2_Φ on circular aperture (exl.piston)

Tilt	Focus	Astigmatisms	Comas	Spherical	residual
87%	2.23%	2.23% x 2	1.2% x 2	0.23%	3.66%

Table 2.7 Vision quality for different atmospheric conditions

D / r_0	$\sigma^2_\Phi = 1.03 \cdot (D / r_0)^{5/3}$	$S \approx e^{-\sigma^2_\Phi / 2}$	S, compensated T + F + A	S, compensated T + F + A + C + Sph
1	1.0299	0.598	0.968	0.981
2	3.27	0.194	0.902	0.942
5	15.057	$5\ 10^{-4}$	0.623	0.753
10	47.81	$4\ 10^{-11}$	0.222	0.417

This figures show that compensation of the second order aberrations can significantly improve the vision quality for small (1 - 1.5 m) telescopes at average values of r_0 about 10 - 20 cm. For the same values of D/r_0 we can calculate the desired deformations of adaptive mirror surface to correct these second order aberrations - see table 2.8. In this calculations we used the relation $Dx=3\sigma\Phi$ that means that for normal distribution of aberrations in 95% of time
wavefront distortion p-p value will be in the range ($-3\sigma\Phi$.. $+3\sigma\Phi$).

Table 2.8. Desired profile deformatons in micrometers (for 95% probability)

D / r_0	1	2	5	10
$\Delta x \approx \frac{\lambda \cdot 3\sigma_\Phi}{2\pi};(\lambda = 2\mu M)$	0.97	1.73	3.71	6.6
Δx TILT	0.9	1.61	3.45	6.14
Δx FOCUS, ASTIGMATISM	0.15	0.26	0.56	0.99
Δx PURE COMA	0.11	0.19	0.41	0.73
Δx SPHERICAL	0.05	0.08	0.18	0.32

The greatest desired value is about 1 μm for the second order aberration deformation. The same is for coma. These results enable us to hope that the mirror investigated can be used successfully to compensate atmospheric turbulence.

2.3. ***Temperature stability***. The temperature stability of the mirror parameters is of great importance for the real applications. In the room where interferometer is installed (it is small enough) we use the simple heat gun for increasing the temperature in the range of a few ^{o}C degrees. For temperature measurements digital thermocouple type thermometer Thandar TH302 was used (precision 0.1 ^{o}C). The thermocouple was attached to the mirror mount.

At fig.2.9 the interferogram and topography of the mirror are shown for temperature values 18^{o}C and 22.6^{o}C. This figures shows significant temperature-defocus dependence due to bimorph structure "glass plate - piezoceramic actuator disk" as well as to the difference in temperature expansion coefficients of the glass and piezoceramics which were used to fabricate the mirror.

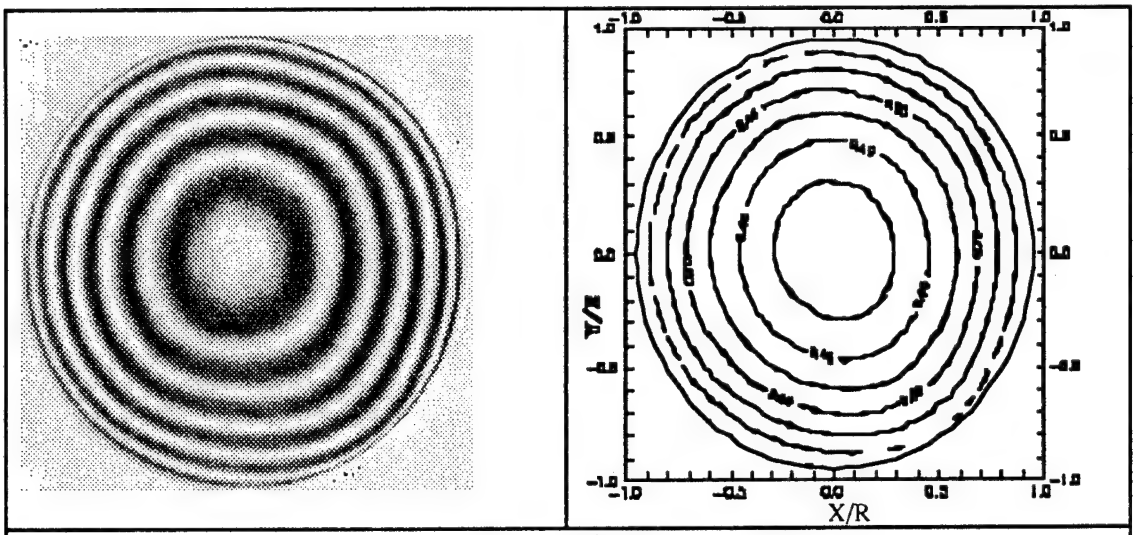

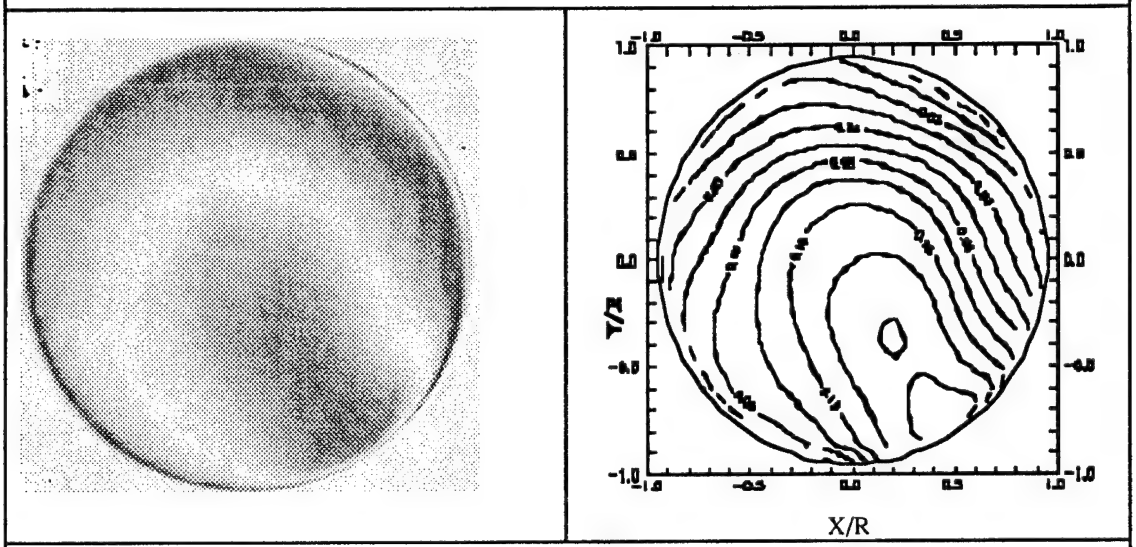

Fig. 2.9. The interferogram and topography of the mirror for 2 temperature values

The temperature dependencies of aberrations in terms of p-v values are represented at fig.2.10. To match the experimental results the linear LSE approximation was used. The most significant value for temperature dependence coefficient was measured for defocus - 0.38 μm/°C, while coefficients for others low order aberrations are 10-30 times less.

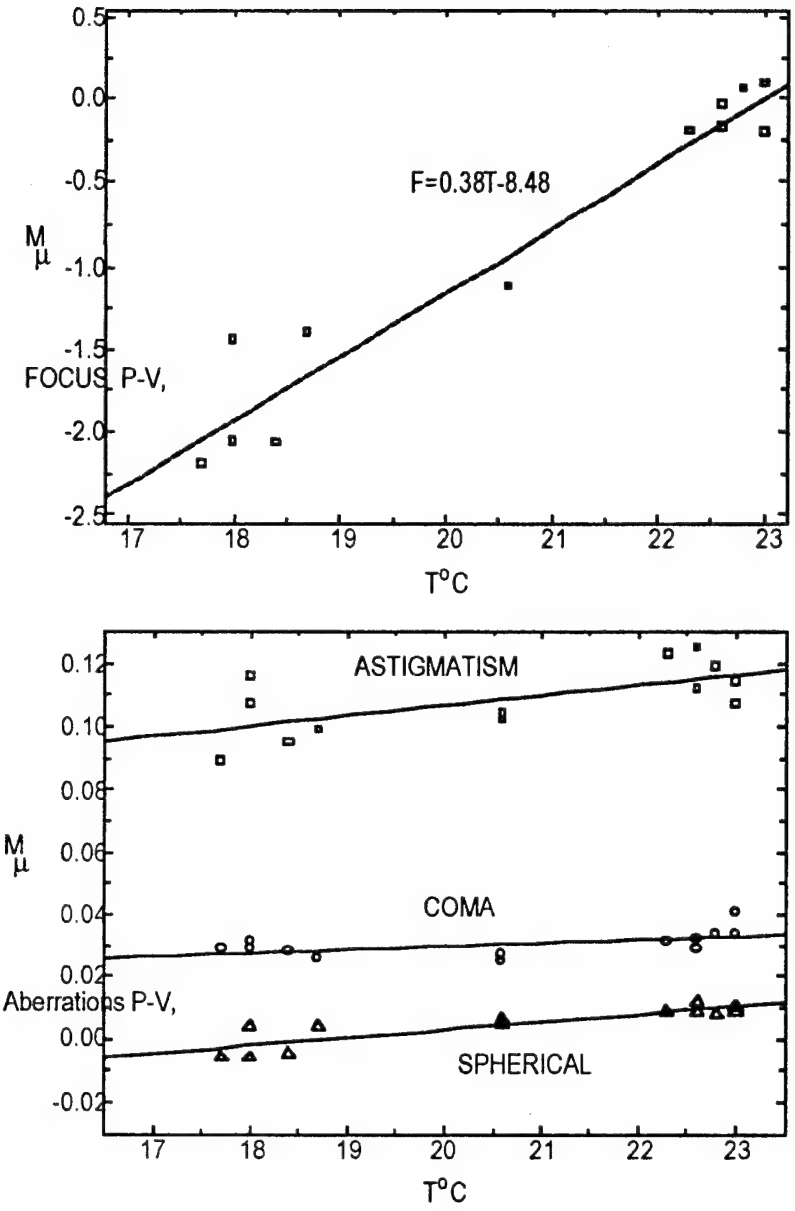

Astigmatism: **0.003·T+0.04** **Coma:** **0.0011·T +0.008** **Spherical:** **0.0025·T - 0.047**

Fig.2.10. Temperature dependencies of the lowest aberrations.

As we can see from results presented in previous sections, the range of aberration control for this mirror is high enough to correct turbulence induced distortions and to compensate its own thermal distortions at 10-15°C variations of temperature.

3. Temporal parameters.

The resonance frequencies of the mirror was measure with the help of Kenwood AG-204 oscillator, ISO-Tech ISR-620 oscilloscope and Black Star Apollo-10 frequency meter. During the measurements we connected driving sine voltage to X input of the oscilloscope as well as to frequency meter while the signal measured was gone to the Y input of the oscilloscope. This enabled us to use both phase and amlitude measurements of resonances that was more precise than pure amplitude measurement.

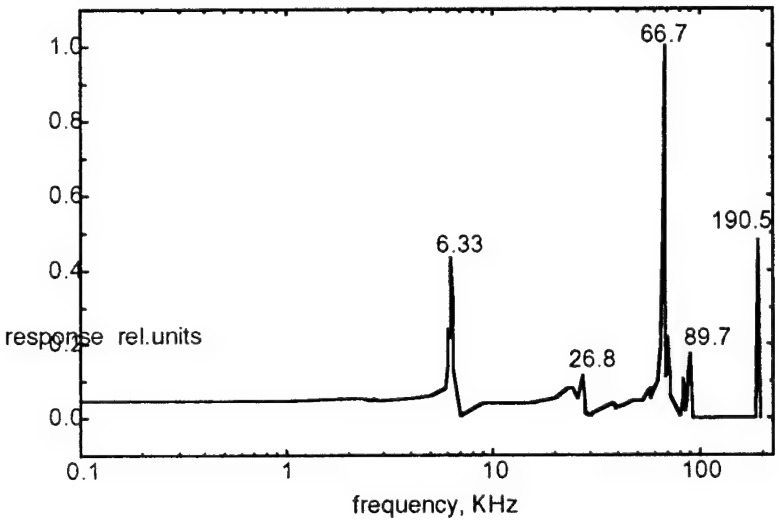

Fig.3.1.

The frequency response curve shown at fig.3.1 was obtained by applying AC voltage to e9 electrode (general focus), output signal was measured on e1 electrode. Similar curves for the case when driving voltage was applied to the e1 electrode and response was measured at one of another segmented electrodes are shown on fig.3.2.

The lowest resonant frequency of the mirror is about 6 KHz, while small peak at 2.5 KHz - (see fig 3.2c) may be caused by the resonance of the mirror attachment plate.

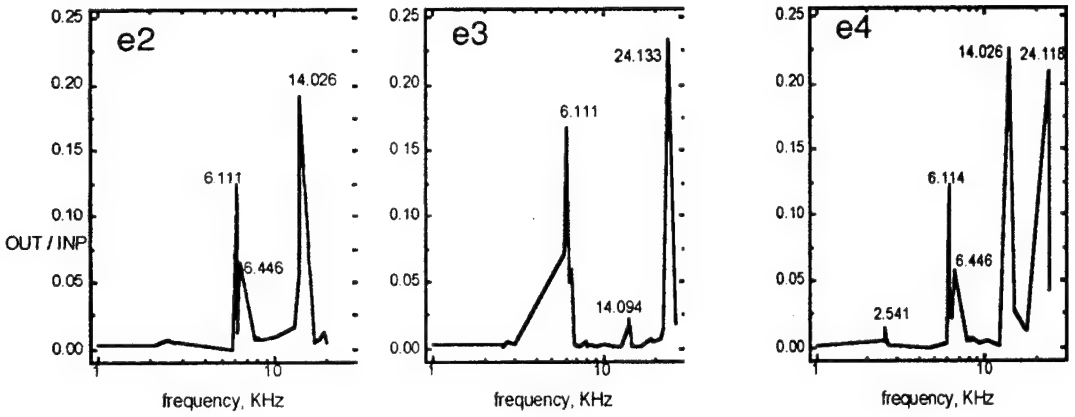

a b c

Fig.3.2

We can conclude that the mirror has operating frequency range up to about 1 KHz, what is sufficiently enough for astronomical applications.

4. Low order adaptive system performance

4.1. ***Experimental set-up.*** In order to illustrate the operation of the BDM we constructed a simple adaptive system for imaging trough laboratory generated turbulence. Experimental set-up of the low-order adaptive system is shown at fig.4.1. The beam of He-Ne laser with 10 mW output was expanded from 1mm to 10mm width by lenses L1 and L2 and directed into the glass water cell, that was used to produce turbulent distortions of the wavefront. The turbulence was produced by convection movement of water between the bottom hot metal plate and the cold one placed at the top of the cell. After plane mirror M1 one part of the beam went through the lenses L5,L6 at the BDM surface. The beam width at the mirror surface was 35mm. After reflection this beam was directed in the "adaptive" measuring arm where lenses L3(F=200mm), 25 μm pin-hole D3 and photodiod PD_1 were used to measure Strehl criterion of the corrected beam.

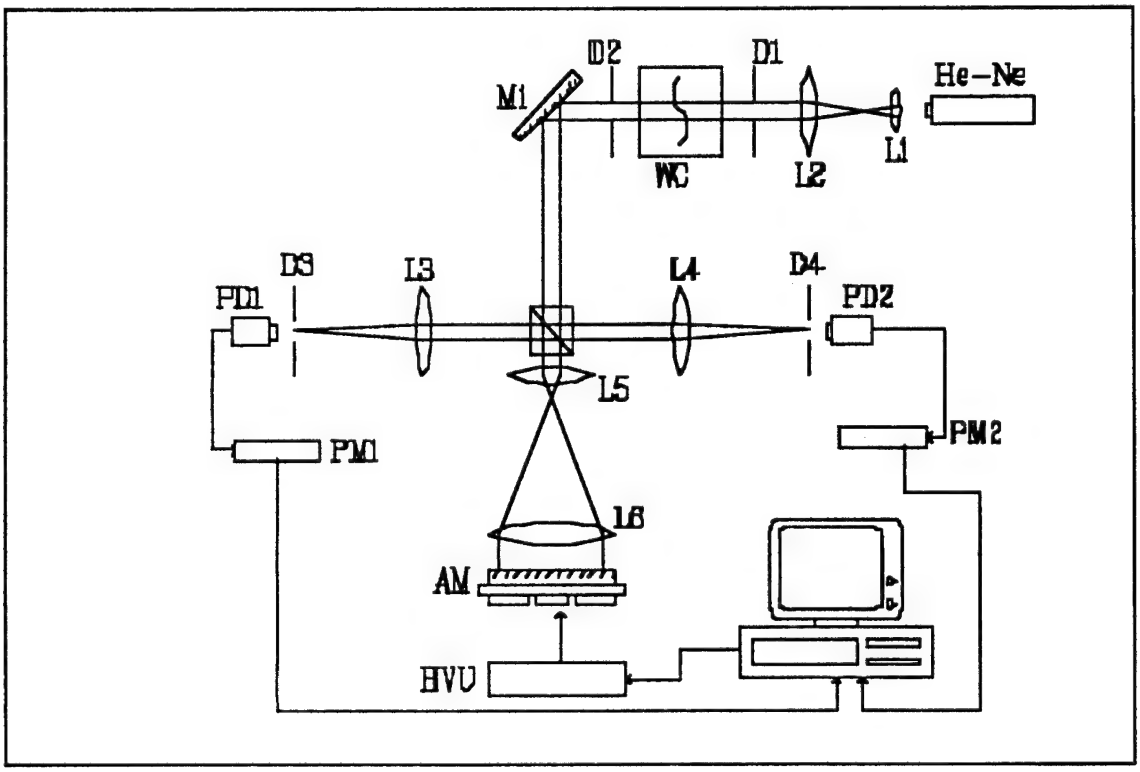

Fig.4.1. Adaptive system experimental set-up.

Another part of the laser beam was gone by the beam splitter directly into measuring arm, containing the lens L4(F=200mm), 25 μm pin-hole D4 and photodiod PD_2, that were used to observe beam quality - axis intensity without phase correction. In order to get the measured criteria - PD_1 and PD_2 signals, the PCL812PG card was used. The ADC circuit on this board has 8 analogue inputs, 12 bits range with programmable input range 0.3125, 0.625, 1.25, 2.5 and 5 V (amplitude). The maximum rate of ADC conversion is 25 KHz. It also allowed us to check the program and hardware delay in the circuit photodiod - ADC - computer - mirror with onboard clock oscillator with accuracy 0.5 msec.

For mirror control we used a DAC unit with 11 output signals and DC Amplifiers with 150V amplitude output. The computer used to control the experimental set-up was Dell PC 486 type, 66 MHz, 8 Mb RAM. The software for our experiment was written on Borland Turbo Pascal 7.0 and gave us possibility to get and to observe the PD_1 and PD_2 signals, to control the mirror and store the data on hard disk. We used the simplest "hill-climbing" [11] algorithm to calculate our control signals for maximisation of the measured criterion.

4.2. ***Turbulence in the water cell.*** Experimental data for two-point coherence function of spherical in the water cell were obtained by A.Bogaturov and V.Myakinin from Institute of Physics of atmosphere, Moscow in the following way.

A point source of spherical wave (focused laser beam) was installed at distance 1 m from the turbulent cell and at distance 2 m from the receiving lens. (To obtain coherence function for a plane wave it is necessary to divide the distance by 2). Average images of this source were captured in the

conjugated plane in the absence of turbulence and in presence of turbulence. The window of CCD-device was wide open and, consequently, these images were the integrals of intensity distribution over the length of one pixel (2.5 μm) rather than intensity distributions. This approach allowed us to obtain coherence function using one-dimensional fast Fourier transformation (FFT). The plot of this coherence function is shown on fig.4.2.

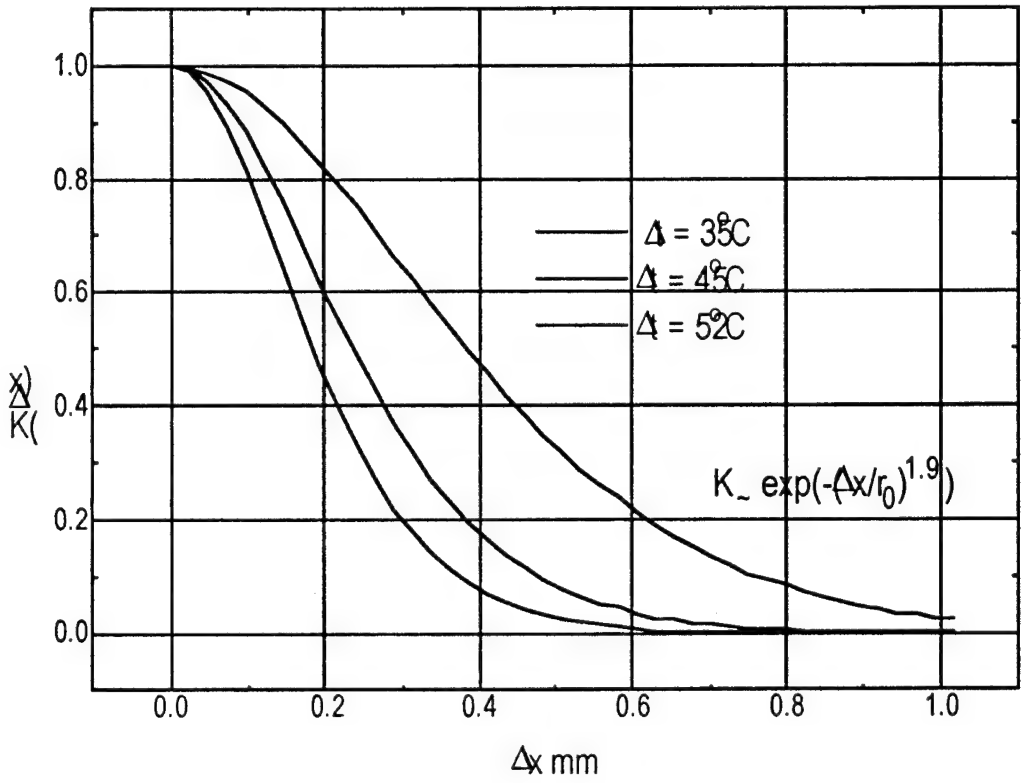

Fig.4.2.Two-point coherence function of spherical wave;
Δt - temperature difference between cold and hot plates.

Assuming that the two-point coherence function may be presented in the following form: $C(r) = \exp(-(r/r_0)^{\alpha})$, and using least-squares method, we may conclude from these data that α approximately equals to 1.9 for all three cases of temperature difference.

In our experiments with adaptive system the temperature difference between cold and hot plates was 30-35°C and r_0 was approximately 0.2 - 0.5 μm.

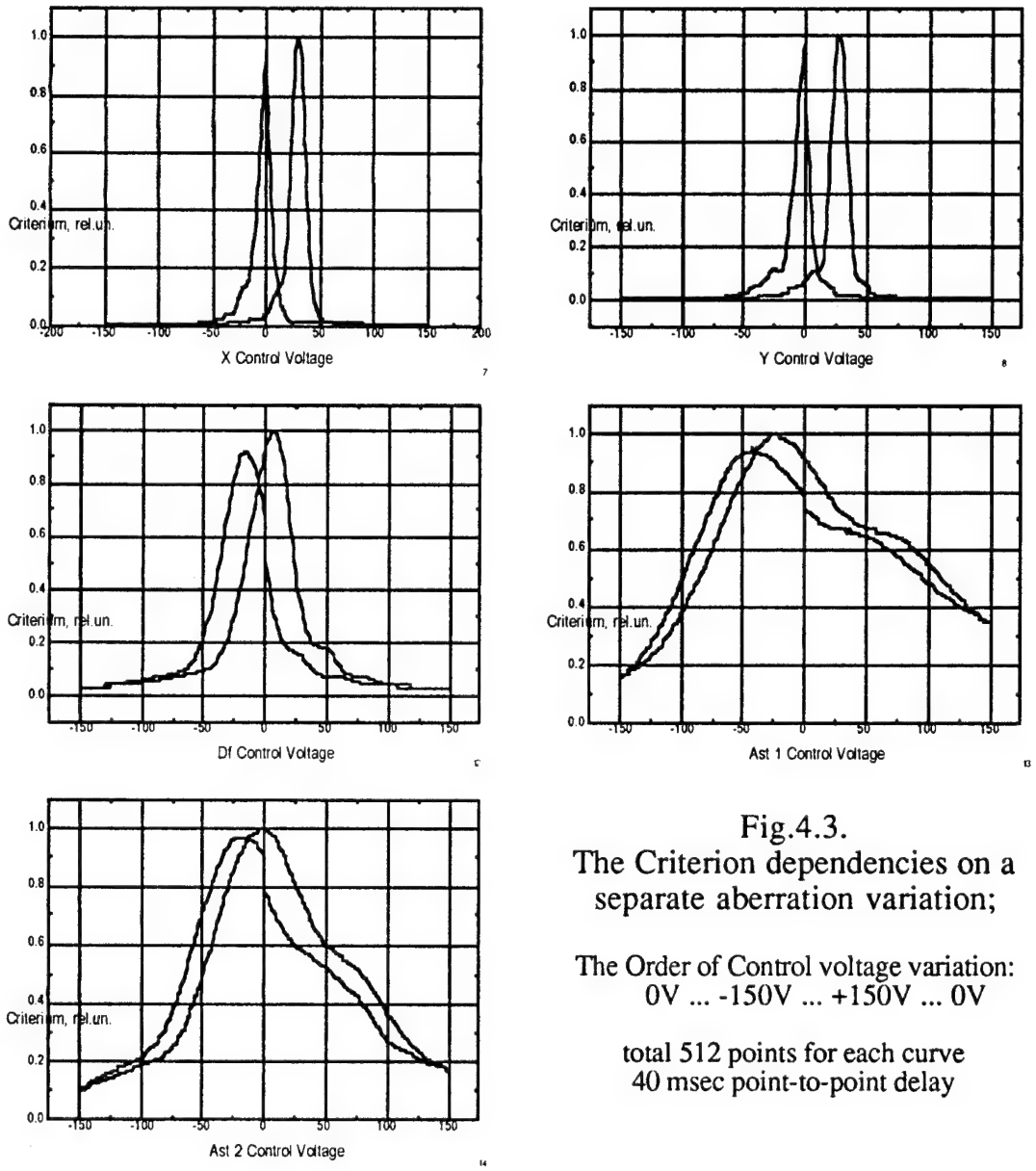

Fig.4.3.
The Criterion dependencies on a separate aberration variation;

The Order of Control voltage variation:
0V ... -150V ... +150V ... 0V

total 512 points for each curve
40 msec point-to-point delay

4.3. ***Controllability***. In order to estimate the controllability of the system at the first stage we measured the influence of the BDM profile variations on the beam quality criterion - PD_1 signal (with no turbulence). These curves for X,Y, defocus and astigmatisms control voltage variations are

shown at fig 4.3. On These curves reveals the strong influence of tip-tilt actuators hysteresis, that is much less for defocus and astigmatism cases. We can consider these curves as 2-D cross sections of the beam quality criterion in 5-D space with X,Y,Df,Ast1 and Ast2 coordinates.

4.4. ***Correction of static aberrations.*** At the second stage of experiments we checked the closed loop system performance for correction of static aberrations - with no turbulence.

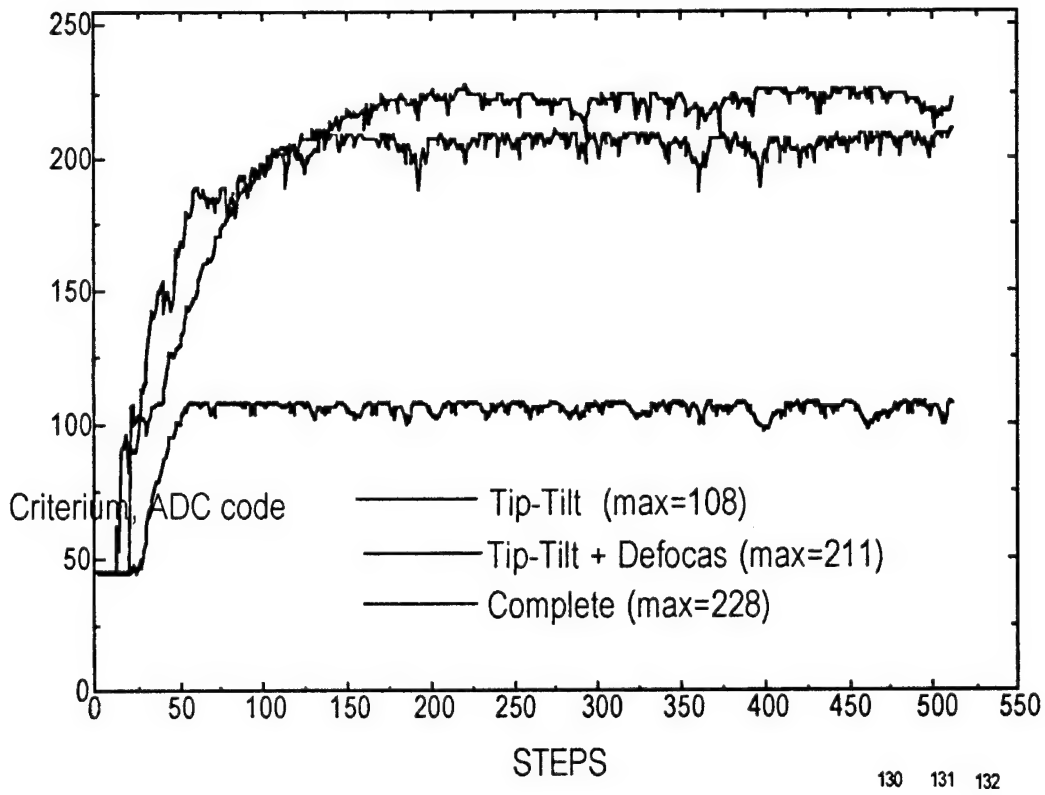

Fig.4.4. The correction of the static aberreations.

First the optical set-up was completely adjusted and the value of our PD_1 signal was measured. Then some static aberrations were imposed by small longitudinal and transverse displacements of the measuring diaphragm D3. So the diaphragm was slightly shifted across the focal spot, by this way we

simulated tip and tilt, and along the beam axis, that gave us defocus aberration. Actually due to a certain misalignments in the optics we obtained not only tip-tilts and defocus but some others aberrations as well. After that the system started to correct the imposed aberrations. As we didn't need high speed performance we set 20 msec step-time.

The typical time dependence of the PD_1 signal during adaptation process is shown on fig.4.4. As we might expect the maximum value of the criterion achieved by adaptation varied as we controlled the different number of aberrations. So the final PD_1 value for only tip-tilt correction was 108, for tip-tilt and defocus - 211, and for tip-tilt, defocus and astigmatisms correction - 228. Initial PD_1 value (before aberrations was imposed) was 225 and it was 48 after aberrations were produced (just before adaptation process started).

As we can see from these data it took the system from about 50 steps (for tip-tilt case) to about 150 steps (for 5 aberrations control) to achieve the maximum of the criterion. The small variations of the PD_1 signal after the system had reached the maximum were due to permanent "checking up" variations of the control signals in accordance with the "hill-climbing" method [11].

4.5. ***Correction of turbulence.*** The temporal and spatial parameters of the turbulence produced in the water cell strictly corresponded each other - when the coherence length r_0 was large the typical value of time scale variations was large as well, and when we had the swift turbulence the coherence length was small. The defraction length for turbulence induced phase distortions r_0^2/λ for r_0=0.5mm, λ=0.63μm had the value about 40 cm. It means that phase distortions in the mirror plane (as well as in the measuring plane) had been transformed into intensity distortions and couldn't have been completely corrected.

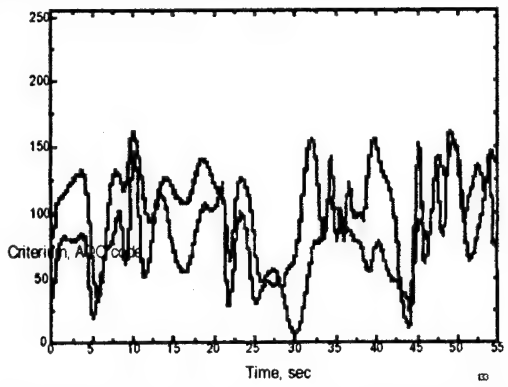

No Adaptation Experiment #133
Cycle Time: 2.6 msec
$<PD_1>$ = 89 ; $<PD_2>$ = 93
Strehl: 0.39 0.41
Correlation: 0.352

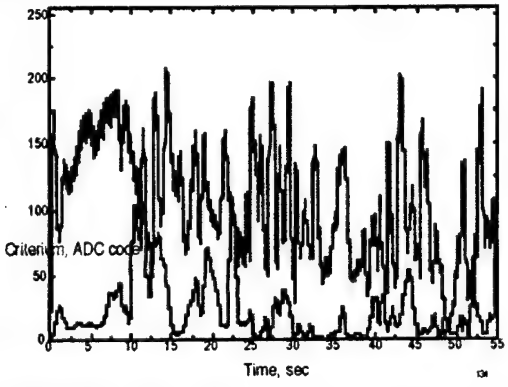

Tip-Tilt Adaptation Experiment #: 134
Cycle Time : 2.7 msec
$<PD_1>$ = 107 $<PD_2>$: = 22.
Strehl: 0.47 0.098

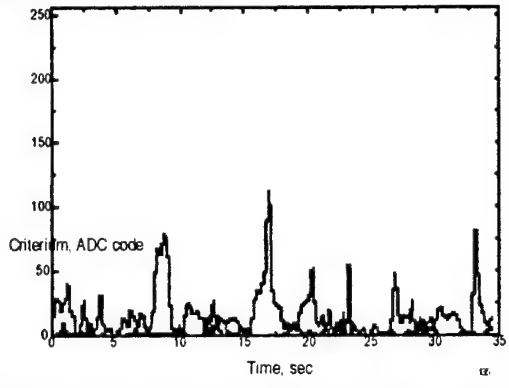

No Adaptation Experiment #: 135
Cycle Time : 1.6 msec
$<PD_1>$ = 29 $<PD_2>$ = 16
Strehl: 0.13 0.065
Correlation: 0.271

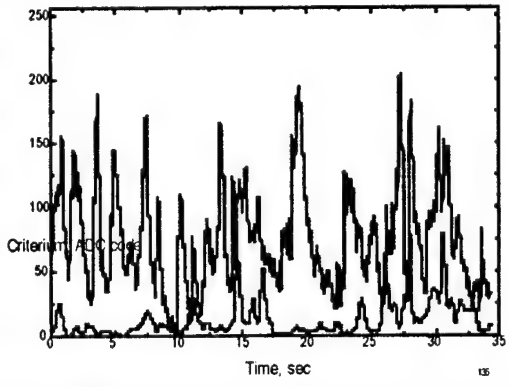

Tip-Tilt Adaptation Experiment #: 136
Cycle Time: 1.6 msec
$<PD_1>$: 76 $<PD_2>$:= 13
Strehl: 0.33 0.053

Fig.4.5 Tip-tilt correction of laboratory induced turbulence;
PD_1 - signal after Water Cell + Adaptive mirror (solid curves)
PD_2 - signal after Water Cell (dashed curves)
$PD_1=PD_2 = 228$ without turbulence

The typical step time delay in the system caused by the software and hardware delays was about 0.6 msec, but to prevent the resonance exitation of the tip-tilt actuators we imposed additional programmable delay in the range 1-2 msec.

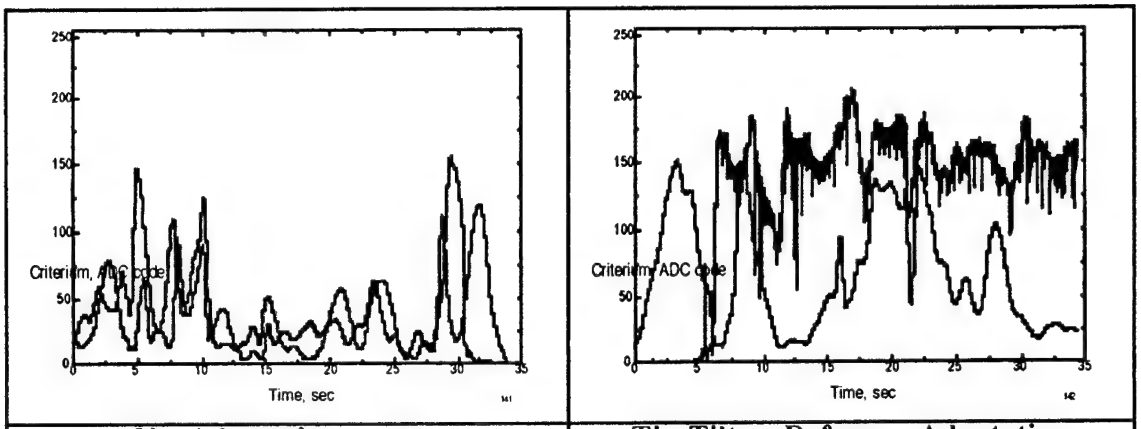

No Adaptation #141
Cycle Time: 1.6 msec
$<PD_1>$ = 32 $<PD_2>$ = 42
Strehl : 0.14 0.18
Correlation: 0.194

Tip-Tilt + Defocus Adaptation
#142
Cycle Time : 2.7
$<PD_1>$ = 125 $<PD_2>$ = 66
Strehl: 0.55 0.29

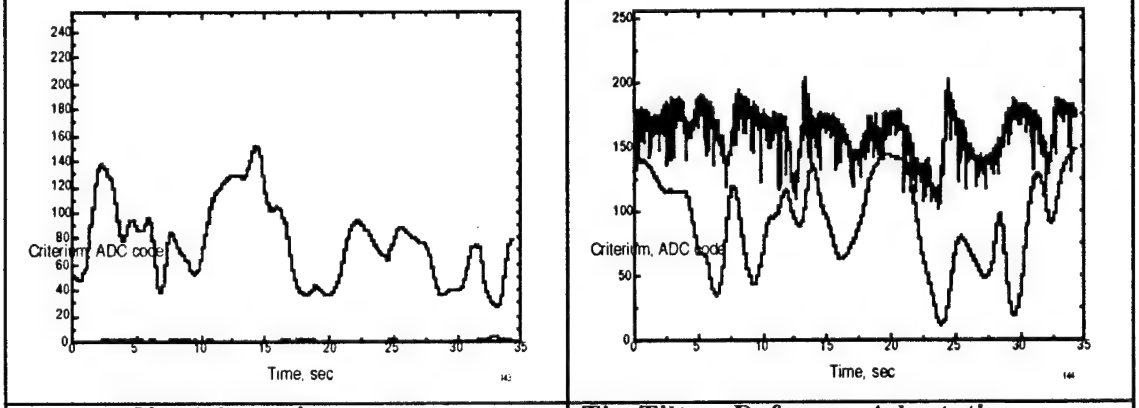

No Adaptation #143
Cycle Time : 1.6 msec
$<PD_1>$ = 1 $<PD_2>$ = 77
Strehl : 0.005 0.34
Correlation: -0.094

Tip-Tilt + Defocus Adaptation
#144
Cycle Time: 1.6
$<PD_1>$ = 161 $<PD_2>$ = 92
Strehl : 0.71 0.40

Fig.4.6 Tip-tilt + Defocus correction of laboratory induced turbulence.
$PD_1=PD_2$ = 228 without turbulence

The performance of the system in the presence of turbulence is illustrated on fig.4.5 (tip-tilt correction only), 4.6 (tip-tilt+defocus correction) and 4.7 (all second-order aberrations). Left columns of these charts show the time dependence of the PD_1 and PD_2 signals (in ADC code units) in opened loop system, and the right columns - in closed loop system.

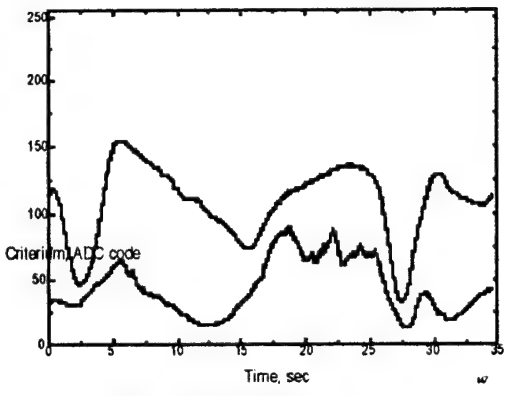

No Adaptation #147
Cycle Time: 1.6 msec
$<PD_1> = 44$ $<PD_2> =$ 108
Strehl : 0.19
0.48
Correlation: 0.454

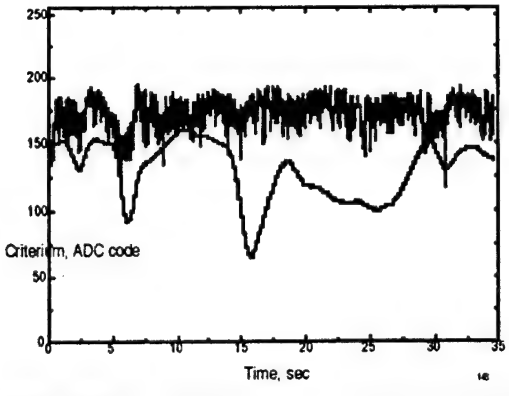

Tip-Tilt + Defocus + Astigmatisms
#148
Cycle Time : 1.7
$<PD_1> = 173$ $<PD_2> =$ 130
Strehl : 0.76
0.57

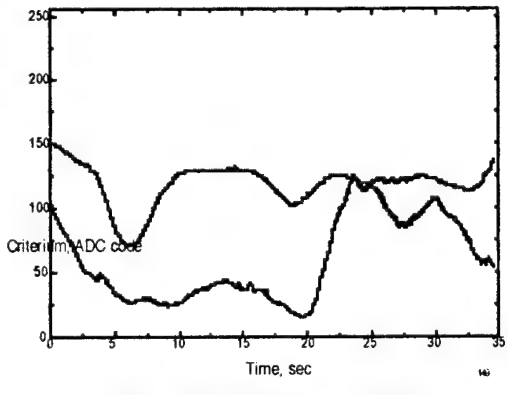

No Adaptation #149
Cyrcle Time : 1.6 msec
$<PD_1> = 12$ $<PD_2> =$ 77
Strehl : 0.005
0.34
Correlation: 0.194

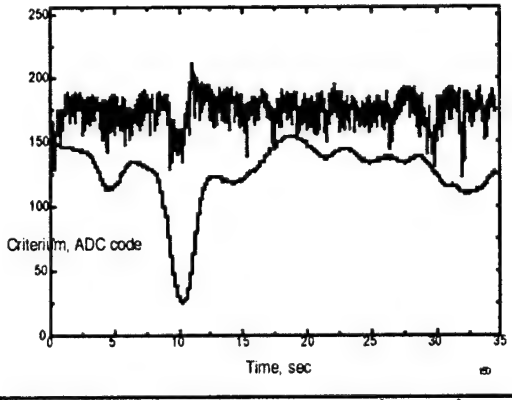

Tip-Tilt + Defocus + Astigmatisms
#150
Cyrcle Time: 1.6
$<PD_1> = 161$ $<PD_2> =$ 92
Strehl : 0.71
0.40

Fig.4.7 Tip-tilt, Defocus + Astigmatisms correction of laboratory induced turbulence.
$PD_1=PD_2 = 228$ without turbulence

Corresponding values of the Shtrehl factor can be calculated by the next formula:

$$S_{1,2} = <PD_{1,2}>/PD_0,$$

where we denoted sample mean value by brackets <...>, and PD_0 is the maximum value of criteria without turbulence. In the described experiments we had PD_0=228.

As we can see in closed loop cases the average values of the "corrected" beam criterion - PD_1 were higher than that of the "uncorrected" beam criterion - PD_2. The comparative values of the S_1 and S_2 as well as their standard deviations σ_1 and σ_2 are shown in the table 4.1.

Table 4.1.

N° of exprmnt	Corrected Aberrations	uncontrolled channel		Adaptive channel		S_1 / S_2	σ_1 / σ_2
		$S_2 = <PD_2>$	σ_2	$S_1 = <PD_1>$	σ_1		
134 - 2ms	tilts	0.10	0.10	0.47	0.20	4.70	2
136	tilts	0.06	0.06	0.33	0.17	5.85	2.8
138	tilts	0.06	0.07	0.32	0.15	5.26	2.1
140	tilts	0.12	0.10	0.39	0.15	3.35	1.5
142	tilts+defocus	0.29	0.18	0.55	0.26	1.89	1.44
144	tilts+defocus	0.40	0.15	0.71	0.08	1.77	0.53
146	tilts+defocus	0.49	0.13	0.73	0.05	1.49	0.38
148	complete	0.57	0.10	0.76	0.05	1.33	0.50
150	complete	0.55	0.11	0.76	0.05	1.39	0.45

The average increase in the Strehl coefficient obtained during the adaptive system performance in our experiments was in the range 1.5-6. We should note that all experiments mentioned in table 4.1 could be subdivided roughly in two groups. In the first group - mainly tip-tilt correction - we had rather great Strehl values increase: from 3.5 to 6, while in the second group - with all second order aberrations corrected (besides tip-tilt) - we had only 1.4 - 1.5 increase. At the same time in the first group we had 2-3 increase of the standard deviations, while in the second group the criterion variance failed in comparison to that of the uncontrolled channels.

The increase of the criterion standard deviation values in the first group can be explained by the sharp dependence of the criterion measured on tip-tilt

changes - see fig.4.3. It means that we had exceedingly large control gain for tip-tilt channels that caused large variances in criterion even at small control signals.

Comparatively small increase in Strehl values in the second group in its turn was due to the increase in the cycle time of the system - as we could see from part 4.4 the typical cycle time for complete aberration control was approximately 3 times greater than that of the only tip-tilt control cases. The decrease in the σ values in this group showed that the weight of the second order aberrations in the beam received was high enough. It enabled us to hope that if we had fast measurements of the beam phase profile we could have much better results on adaptive correction with our mirror.

The next step of this system development could be the additional complete analogue or analogue-digital circuit for tip-tilt correction with rather simple quadrant detector for measurements of the lens's L3 focal spot movement. The final stage would be the adaptive system with Shark-Hartmann wave front sensor with relatively small number of light sensitive subapertures - about 16x16.

5. Conclusions

The main spatial parameters of the mirror investigated are shown in the table 5.1. Here we can see the control coefficient k, the temperature dependence coefficient μ, relative rms of aberration fitting and p-p aberration deformation. The plane fitting rms is about 0.033μM.

Table 5.1. Main parameters of the mirror.

Aberration	*k, μM/V·10²* *exprmnt* *calc*	*at 200 V*	*RMS/P-V %*	*μM/1°C*
Focus	2.56	5.1	0.6	0.38
Astigmatism	2.06	4.1	3	0.003
Pure Coma	0.51	1	5 - 15	0.0011
Spherical	0.1	0.2	30	0.0025

The typical width of the mirror's actuator hysteresis curve is about 10% while operating frequency is almost 1KHz.

We had built-in the mirror in the simple hill-climbing adaptive system for compensation of the laboratory induced turbulence. The performance of this system showed the possibility to improve beam quality in presence of strong turbulence - with D/r_0 values about or greater then 10. In this closed loop system we achieved 1.5-6 increase of the Strehl parameter.

6. Acknowledgements

The authors are glad to express their gratitude to optical engineer F.Reavell, Dr.A.Cañas, electronics engineer S.Hanif and other Applied Optics group staff members for help and assistance.

7. References

1. R.Q.Fugate, Laser beacon Adaptive optics, Conf."Adaptive optics and laser beacons", Brighton, 14 Apr, 1994.

2. M.A.Vorontsov, A.V.Kudryashov A.V.Nazarkin, V.I.Shmalhausen , Sov.J. Quantum.Electron. Vol.11, No 6, 1984.

3. M.A.Vorontsov, A.V.Kudryashov, V.I.Shmalhausen. Sov.J. Izvestija VUZov (Reports of the USSR High School) - RadioPhysics, Vol.27, No 11,1984.

4. M.A.Vorontsov, A.V.Koryabin, V.I.Shmalhausen. Sov.J. Izvestija VUZov (Reports of the USSR High School) - RadioPhysics, Vol.27, No 3,1984.

5. M.A.Vorontsov, A.V.Koryabin,V.I.Polezhaev, V.I.Shmalhausen , Sov.J. Quantum.Electron. Vol.18, No 8, pp.904-905, 1991.

6. A.Abbas, L.N.Kaptsov, A.V.Kudryashov et al. Sov.J. Quantum.Electron. Vol.19, No 6, p.581, 1992.

7.G. Rousett, Slope and curvature sensor based Adaptive Optics system..Conf.: "Adaptive optics and laser beacons", Brighton, 14 April 1994.

8. S.A.Kokorowsky, JOSA, Vol.69, pp.181,1997.

9. S.G.Lipson, E.Steinhaus, JOSA, Vol.69, pp. 478, 1979.

10. R.J.Noll, JOSA,v.66,3,207-211(1976).

11. J.W.Hardy, Proc.IEEE, Vol.66, No 6, pp.651-697,1978.

12. M.A.Vorontsov, A.V.Koryabin, V.I.Shmalhausen. Control in Optical Systems. Nauka publ., Moscow, 1988.